MALAYSIAN JOURNAL OF SCIENCE
MJS
ISSN 1394 - 3065

FAST-UTHM Global Nexus Conference 2024

Special issue

Malaysian Journal of Science 45 (Special Issue 1): 37-43 (June 2026) https://mjs.um.edu.my

Mode-Locked Based on Side-Polished Fiber Coated with Gold as a Medium for the Temperature Sensor

Noor Azura Awang[1a]* and Nik Noor Haryatul Eleena Nik Mahmud[2b]

Abstract: We present a mode-locked based on side-polished fiber (SPF) as a medium for temperature sensing. To develop a mode-locked fiber sensor (MLFS), an erbium-doped fiber and gold nanoparticles with 10 nm thickness were coated onto SPF. An MLFS pulse was generated at 38.5 MHz with a pulse interval of 0.0258 µs, matching the cavity round-trip time. The sensing part was tested under two conditions: heating (100 to 0 °C) and cooling (0 to 100 °C). The experiment revealed a linear relationship between the resonant wavelength shift and temperature variations, with sensitivities of 0.4079 and 0.3775 nm °C^{-1} during heating and cooling, respectively. The SNR value increased from 43.9 to 56.3 dB, indicating stable output power precision. Moreover, the incorporation of a gold-nanoparticle coating on SPF improved sensor sensitivity and reliability while reducing the effects of external variables such as moisture and vibration. These properties also describe the sensor's strength and adaptability in demanding industrial and commercial applications. Future research will focus on assessing long-term performance under changing environmental conditions, thereby ensuring dependability across varied contexts.

Keywords: Gold nanoparticle, Fiber laser, Mode-locked, Side-polished fiber, Temperature sensor.

1. Introduction

The characteristics of mode-locked fiber laser (MDFL), such as narrow pulse width, wide spectrum, and high pump power, could lead to potential uses such as environmental sensing, material processing, and medicine (Fried et al., 2005; Li et al., 2022; Stewart et al, 2003; Zhang et al., 2002). A passive MDFL with a saturable absorber (SA) is more effective at generating ultrashort pulses than an active MDFL that employs active modulation. The use of SA changes resonator losses much faster than active electronics. Additionally, it is more economical and compact (Lu et al., 2018). A prior study indicated that pulse fiber lasers effectively achieved operation under the impact of SA, including 2D materials, topological insulators (TI), Semiconductor Saturable Absorber Mirror (SESAM), black phosphorus (BP), and transition metal dichalcogenides (TMD) within the laser cavity (Jung et al., 2014; Matsas et al., 1992; Novoselov et al., 2005; Song et al., 2017; Trushin et al., 2016). However, some SA materials have severe limitations, including low stability and performance, a low damage threshold, and a narrow operating wavelength (Keller, 2004). Recently, Guo et al. and Ahmad et al. reported their work using silver nanoparticles (SNPs) because SA can produce pulsed fiber lasers. Thus, this suggests that transition-metal exploration includes silver and gold, as SA has emerged as a new approach to ultrashort-pulse lasers due to its unique optical properties (Liao et al., 1997; Zhou et al., 1994).

Recently, fiber laser temperature sensors have attracted significant attention from researchers due to their high sensitivity, high signal-to-noise ratio (SNR), ease of manufacture, and good anti-interference performance (Madry et al., 2019; Gonzalez-Reyna et al., 2015). Numerous optical fiber sensors operating at 1.5 µm have been demonstrated, largely because of the superior quality and broad availability of components in the C-band. For example, optical fiber including fiber Bragg gratings (FBGs) (Lin et al., 2015), long-period fiber gratings (LPGs) (Viegas et al., 2009; Fu et al., 2020), Sagnac interferometers (SI) (Chen et al., 2018), and photonic crystal fibers (PCF) (Luo et al., 2021). However, some of the technologies have inherent drawbacks. Standard FBGs etched with UV lasers may exhibit reduced reflectivity and increased brittleness at high temperatures, especially above 300 °C (Wu et al., 2015; Wang et al., 2022). The Michelson interferometer with misaligned fibre requires additional adjustments or calibration during construction, which increases complexity (Cao et al., 2017), in contrast to the Fabry-Perot interferometer with air cavities, which may be insensitive to temperature variations (Lu et al., 2023).

Furthermore, new developments in the production of fibre Bragg gratings using femtosecond laser pulses have removed several constraints. Femtosecond laser-induced fibre Bragg gratings are more heat-resistant and more stable compared to their UV-inscribed equivalents. Based on the research conducted by Grobnic et al. (2006), it is possible to permanently alter the refractive index by a factor of up to 10^{-3}. Grobnic et al. (2006) have found that Type-II FBGs made of SMF-28 fibres may resist

Authors information:
[a]Faculty of Applied Sciences and Technology (FAST), Universiti Tun Hussein Onn Malaysia (UTHM), Pagoh Branch Campus, Pagoh Higher Education Hub, Km 1, Jalan Panchor, 84600 Muar, Johor Darul Ta'zim, MALAYSIA.
E-mail: norazura@uthm.edu.my[1]
[b]School of Physics, Universiti Sains Malaysia, 11800 USM, Penang, MALAYSIA.
Email: niknoorharyatuleleena@gmail.com[2]

*Corresponding Author: norazura@uthm.edu.my

Received: May 25, 2025
Accepted: July 30, 2025
Published: June 30, 2026

DOI: https://doi.org/10.22452/mjs.vol45sp1.5
Malaysian Journal of Science 45 (Special Issue 1): 37-43 (June 2026)

temperatures as high as 1000 °C (Grobnic et al., 2006). Therefore, the use of femtosecond pulses offers a reliable solution for high-temperature sensing, thereby expanding their usefulness in very demanding conditions.

In addition to FBGs, other fiber-optic-based temperature sensors have also been studied. A biconical fiber temperature sensor has previously been investigated, which had temperature sensitivities of 0.010 and 0.0067 nm °C^{-1} for tapered lengths of 20.548 and 18.382 mm, respectively (Kieu & Mansuripur, 2006). However, these geometries have some disadvantages, including susceptibility to low temperatures and the need for complex processing techniques. In contrast, side-polished fibers (SPF) are among the most attractive alternatives because their cores are exposed, enabling strong evanescent-field interaction with external media. Because of this kind of interaction, SPF structures are very responsive to changes in the external refractive index and temperature. Previous work has shown their efficiency in improving the performance of relative humidity sensors (Huang et al., 2018), refractive index, and temperature (Teng et al., 2022). Their versatility suggests the possibility of enhancing sensing applications involving temperature and the environment using a simpler geometry than configurations such as FBGs.

In addition, SPF offers several advantages over etched, tapered, or LPFG structures, including low attenuation losses, cost-effectiveness, ease of fabrication, and mechanical robustness (Arjmand et al., 2017). To perform MDFL, the SPF has been coated with metal nanoparticles such as gold nanoparticles (NP) (Mahmud et. al., 2023). Since gold-NP shows a higher value of the third-order non-linear coefficient than that of other nanomaterials, it is a suitable material to be used as an SA for pulse generation (Liao et al., 1997).

In this study, we constructed a mode-locked fiber sensor (MLFS) incorporated into an EDFL cavity to produce pulses for temperature measurement. Compared with the femtosecond laser-inscribed FBG, this solution does not require an expensive ultrafast inscription system while still offering high temperature sensitivity and strong signal-to-noise performance enabled by mode-locking. The entire laser cavity consists of 0.5 m of EDF with an overall length of 2.81 m. The gold-NP SPF serves simultaneously as a saturable absorber and a temperature-sensitive element with sensitivities of 0.4079 (cooling) and 0.3775 nm °C^{-1} (heating). This simple, low-cost arrangement demonstrates the capability of SPF-based structures for scalable, practical optical fiber temperature sensors.

2. Experimental setup

2.1 Side-Polished Fiber-Coated Gold

The fabrication of gold thin film is shown in Figure 1 by using the Quorum DC magnetron sputtering technique. To begin the procedure, the chamber was filled with argon gas to achieve a complete vacuum. This process enabled the ionized Argon gas atoms to collide with the gold target, therefore releasing the particles into the existing plasma. Thus, the negatively charged gold atoms are moved into a positively charged substrate and then condensed, forming a thin layer. Before starting the deposition process, the density was set at 19.32 $gm^{-3}$with a thickness of 10 nm. The distances of core and cladding after deposition were 93.239 and 245.811 µm.

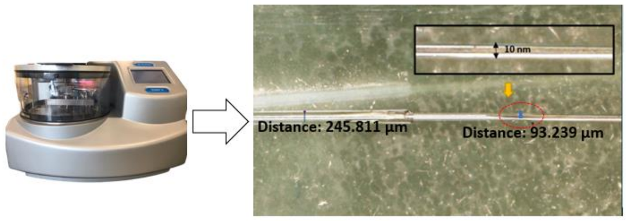

Figure 1. SPF coated with gold using a Quorum DC magnetron sputter coater.

2.2 Temperature Sensor

Figure 2 shows a single-ring cavity that includes 32.12 dBm^{-1}absorption coefficient of 0.5 m EDF with overall length cavity 2.81 m (Mahmud et al., 2022). This setup operates with a 980 nm laser diode (LD). To prevent unidirectional light transmission within the laser cavity, an isolator was used in the setup. A wavelength-division multiplexer (WDM) was used to combine and separate light into distinct wavelengths. The laser output was extracted through a 10% fiber coupler, while the remaining 90% circulated within the cavity. To generate MDFL, a gold-NP SPF was integrated in the setup, and 50% of the laser output was monitored by an optical spectrum analyser (OSA) and an oscilloscope (OSCI). The gold-NP SPF, which served as the sensor, was submerged in water, and a thermometer was inserted to measure the temperature. An MFLS was evaluated throughout both the heating and cooling cycles. The water was heated to 100 °C, and after the measurements were taken, the hot plate was turned off to initiate cooling. During heating, the MLFS output pulse varied over the temperature range of 0 to 100 °C; during cooling, it varied from 100 to 0 °C.

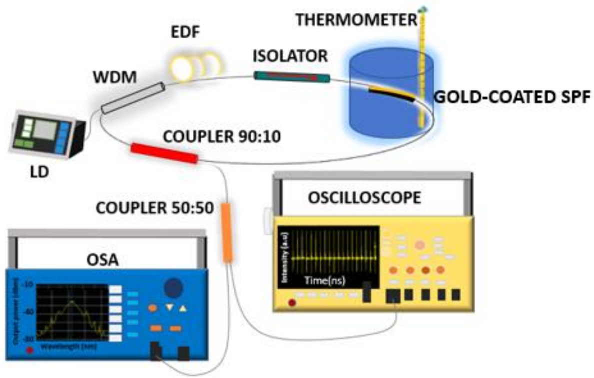

Figure 2. Configuration of mode-locked fiber sensor (MLFS).

DOI: https://doi.org/10.22452/mjs.vol45sp1.5
Malaysian Journal of Science 45 (Special Issue 1): 37-43 (June 2026)

3. Results and analysis

An initial measurement of the optical spectrum of the MFLS at room temperature is shown in Figure 3(a). With a pump power of 297.3 mW, the MLFS optical spectrum has a centre wavelength of 1563.1 nm and a 3-dB bandwidth of 11.2 nm. The presence of Kelly sidebands in the output spectrum was attributed to the abnormal dispersion occurring in the ring cavity (Sun et al., 2010). These sidebands arise from the periodic interference between soliton pulses and dispersive waves circulating in the cavity, confirming that pulse shaping is governed by soliton dynamics. Figure 3 (b) depicts a pulse train of the MLFS operating at a frequency of 38.5 MHz. The pulse interval was determined to be about 0.0258 µs, matching the cavity's round-trip duration exactly. Hence, verifying the mode-locked laser's basic operation.

As shown in Figure 3(c), the pulse width of the MFLS was determined by analyzing the autocorrelation trace and fitting it with a $sech^2$ profile. The blue curves represent the measured autocorrelation (ACF) signal, while the red curves refer to the theoretical fit based on the $sech^2$ temporal profile. From the fitting result, the full width at half maximum (FWHM) of the autocorrelation trace was measured to be 1.149 ps. Assuming the $sech^2$ pulse shape, a deconvolution factor of 1.543 was applied, yielding an estimated pulse duration of 0.691 ps ≈ 691 fs. The MSE of 5.313×10^{-5} indicated excellent agreement between the experimental data and the fitted curve, and hence the generated pulse closely follows a $sech^2$ profile. Furthermore, the narrow autocorrelation width and good fit quality confirm that stable ultrashort pulses were produced by the mode-locked fiber laser.

Figure 3(d) shows that the OSCI captured the RF spectrum of the MLFS, with a 500 MHz scanning span. The inserted image shows that the first-order peak aligns precisely with the laser cavity's repetition frequency, observed at 38.5 MHz. With an SNR of 44.1 dB, this finding indicates that the MLFS is operating steadily. Consistent with the basic cavity repetition rate determined from the OSCI trace, the observed trace generates the fundamental frequency at 3.86 MHz. According to Li et al., the stability and coherence of mode-locked operation were verified by the presence of a clear fundamental peak and the absence of subharmonic components (Li et al., 2023).

After the reference measurements were completed, the water was heated using a hot plate, with measurements taken across the temperature range from 0 to 100 °C. Throughout the experiment, the pump power was maintained at 297.3 mW to ensure consistent results and minimize environmental interference. Figure 4 (a) presents the output spectrum of the MLFS at 0, 40, and 100 °C, as recorded by OSA. At 0 °C, the resonant wavelength was observed at 1530.20 nm. As the temperature increased, the resonant wavelength shifted to longer wavelengths, moving from 1530.20 nm at 0 °C to 1568.70 nm at 100 °C, with a corresponding change in output power from -13.60 to -13.20 dBm. Figure 4(a) shows that 100 °C results in the largest shift among the other temperatures, due to the SPF's thermo-optic behavior (Senosianin et al., 2002). Although the refractive index was not directly measured in this work, temperature-induced changes in the refractive index of the exposed core region are well established in the literature, particularly for structures with strong evanescent-field

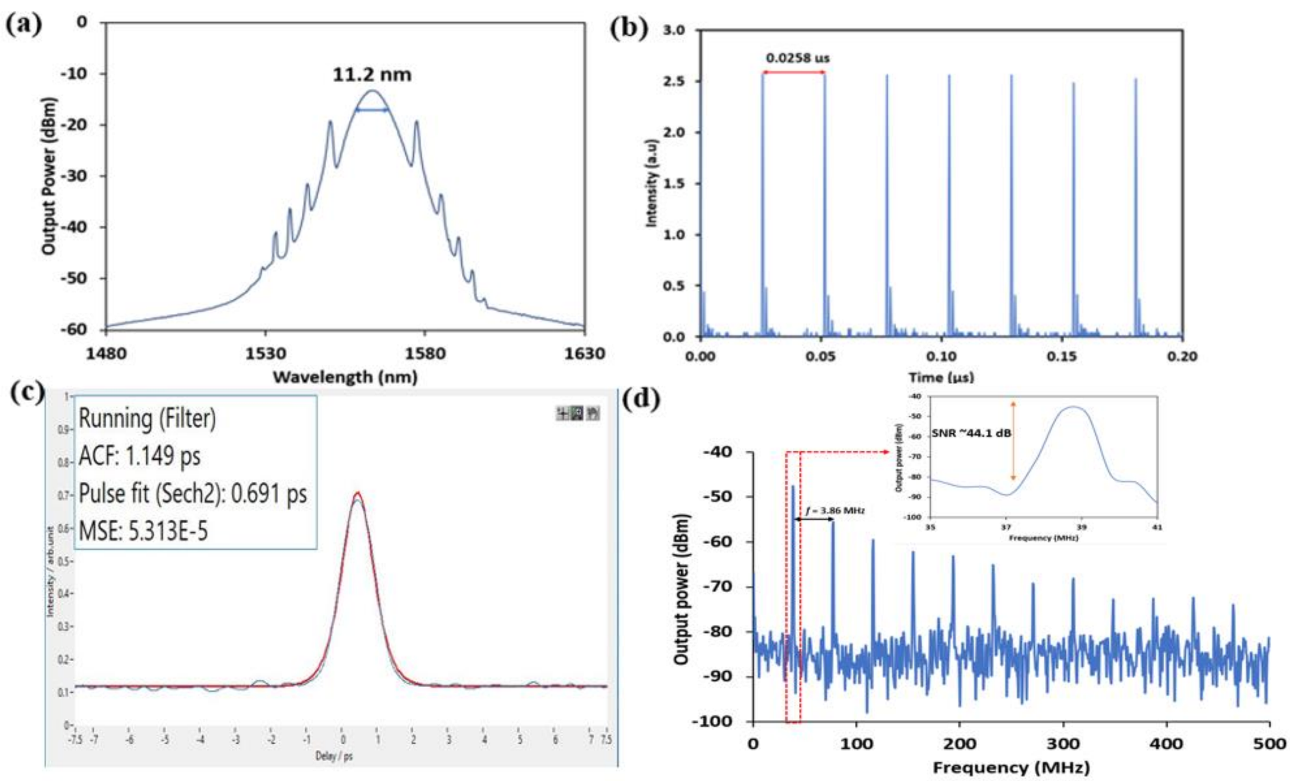

Figure 3. Performance of MLFS (a) Optical spectrum (b) Pulse train (c) Autocorrelation trace (d) Radio-frequency (RF) spectrum

DOI: https://doi.org/10.22452/mjs.vol45sp1.5
Malaysian Journal of Science 45 (Special Issue 1): 37-43 (June 2026)

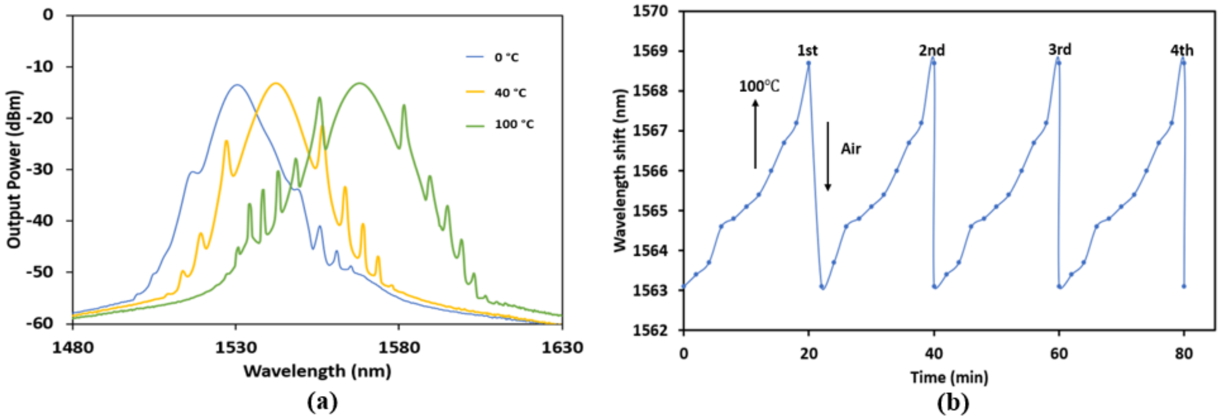

Figure 4. (a) Output spectrum of the MLFS varies at temperatures 0, 40, and 100 °C. (b) Repeatability of wavelength shifting at 100°C temperature.

interactions. Such a thermo-optic effect alters the optical path length of SPF, resulting in a red shift of the lasing wavelength at high temperatures (Zainuddin et al., 2019). Otherwise, temperature-dependent effects have been observed in plasmonic absorption and the non-linear response of the gold-NP coating (Ganeev, 2019). These changes further affect the EDF laser's intracavity gain-loss balance, leading to spectrum broadening and intensity fluctuations in the experiment, which explain the significant temperature-dependent wavelength shifts observed in this work (Jachpure & Vijaya 2024).

Additionally, the gold-coated SPF was monitored at 100 °C (indicated by the upward arrow) for 4 cycles, as illustrated in Figure 4(b). The findings reveal that wavelength shifting from 1563.1 to 1568.7 nm with a tuning range of 5.6 nm. After 20 minutes, the wavelength shift stabilized, and upon exposure to air (arrow downward), the wavelength returned to its reference value within 10 minutes. This behavior was consistent across multiple cycles, even at other temperatures, demonstrating that the sensor has good stability and a fast recovery time in air.

During heating, the OSA obtained the radio-frequency (RF) spectrum of the MLFS, as shown in Figure 5(a). The power and frequency of the MLFS's output are shown in the graph as a function of temperature. The frequency remains constant at 38.5 MHz, whereas the output power drops from -44.74 dBm to -57.21 dB as the temperature increases. At 100 °C, the SNR is 56.30 dB, up from 43.84 dB at room temperature, suggesting a higher SNR even with the pump power unchanged. This increase in SNR is due to the laser cavity being thermally stabilized and to the gold-coated SPF, which introduces improved resonance characteristics.

The temperature was lowered from 100 to 0 °C in 20 °C increments by adding ice cubes throughout the cooling process. Figure 5(b) shows that the RF spectrum produces an output power of -50.83 dBm at 100 °C and gradually increases to -44.76 dBm at 0 °C while the MLFS operates at a cooling temperature. The rate of repetition remains the same throughout the procedure. Although thermal factors throughout the experiment play a

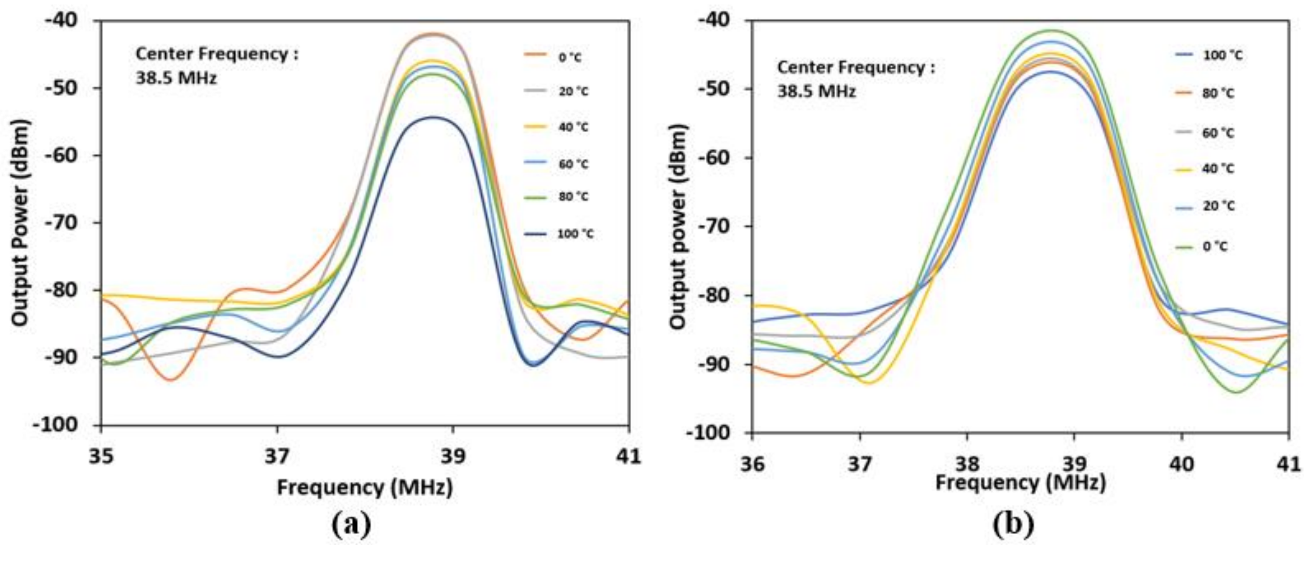

Figure 5. The graph between output power and frequency against temperature for (a) heating and (b) cooling processes.

DOI: https://doi.org/10.22452/mjs.vol45sp1.5
Malaysian Journal of Science 45 (Special Issue 1): 37-43 (June 2026)

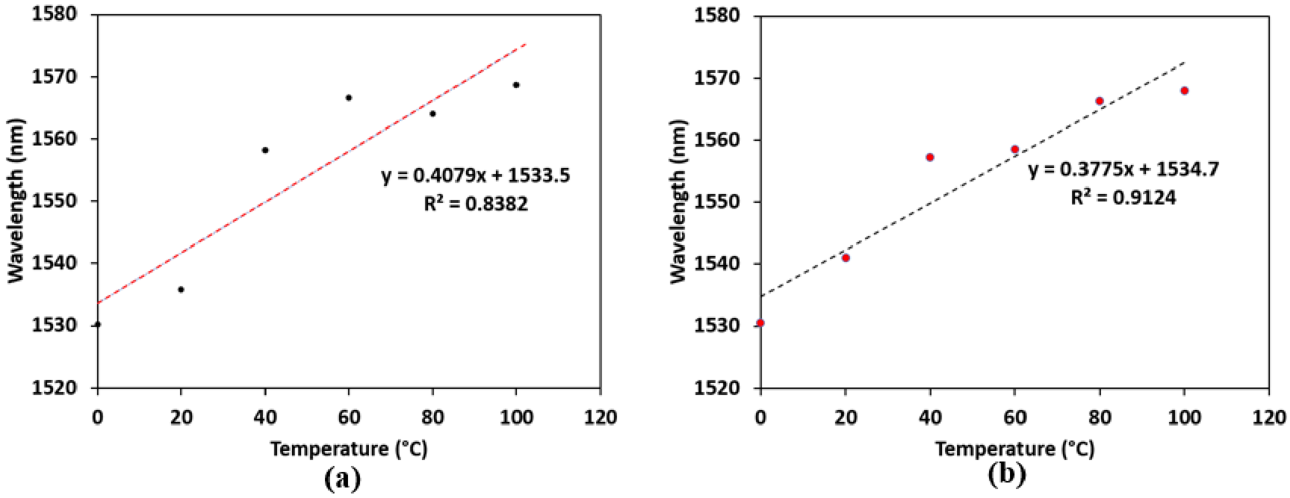

Figure 6. a) Wavelength shift of the MFLS during (a) heating and (b) cooling processes.

secondary role in determining SNR stability, the SNR declined from 50.00 to 43.90 dB during cooling, suggesting that temperature fluctuations had little effect on SNR (Fu et al., 2020). The gold-NP SPF contributes to the higher SNR observed at higher temperatures. According to Chou et al. (2019), this material has superior performance compared to others when it comes to wavelength tuning range, resonance augmentation, and sensitivity (Chou et al., 2019). Incorporating a gold-NP SPF into the laser ring cavity thus significantly enhances the MFLS SNR. To evaluate the sensor's functionality and performance in harsh environments, further research over a wide temperature range is required, even though the present findings demonstrate that the SNR remains generally constant across the observed range.

The data are fit to a linear relationship between the resonant wavelength shift and temperature variation, as shown in Figure 6(a). The graph shows that as temperature increases, the wavelength shifts toward longer wavelengths (Sharma & Gupta, 2006; Bai et al., 2019). This is due to the thermal effect, which causes the resonance wavelength to shift during heating (Chou et al., 2019). Therefore, the wavelength shifts to longer wavelengths during heating. At temperatures higher than 60 °C, there is a non-linear shift in wavelength that is caused by the interplay between the exposed core area of the SPF, the plasmonic and non-linear absorption properties of the gold nanoparticle coating (Ganeez 2019), and the EDF's temperature-dependent gain profile (Bolshtyansky et al., 2000). These factors cause wavelength changes to occur more rapidly at higher temperatures, unlike the usual simple linear thermo-optic behavior observed in FBG-based sensors.

During cooling, the MLFS temperature was slowly reduced to room temperature, then reached 0 °C after some ice cubes were added. In Figure 6(b), the resonant wavelength shifts toward shorter wavelengths as the temperature decreases from 100 to 0 °C. During the cooling process, the temperature decreased, and the resonant wavelength shifted from 1568.00 to 1530.55 nm, so the wavelength shifted by around < 10 nm. Based on Figure 6 (a-b), the temperature sensitivity of the heating and cooling conditions was about 0.4079 and 0.3775 $nm\,°C^{-1}$, indicating a hysteresis of approximately 8% (Lin et al., 2020). This level of hysteresis is considered significant because an ideal temperature sensor should exhibit responses that are almost identical during heating and cooling. The observed divergence suggests that the system does not fully return to its original spectral position after each heat cycle. This conclusion is most likely due to the gold-NP SPF expanding at different rates during heating, potentially resulting in residual mechanical stress at the interface. Each condition yields R^2 value of 0.8382 and 0.9124.

4. Conclusion

In this paper, the successful demonstration of an MLFS coated with gold-NP is presented, with its temperature characteristics thoroughly examined. The sensor exhibits temperature sensitivities of 0.4079 $nm\,°C^{-1}$during heating and 0.3775 $nm\,°C^{-1}$ during cooling, the presence of thermal hysteresis. As the temperature rises, the resonant wavelength shifts toward longer wavelengths, and the experimental data confirm a strong linear correlation between the wavelength shift and ambient temperature fluctuations. In addition, the temperature effect on output power and SNR was examined, showing that an increase in SNR due to the enhanced sensitivity of the gold-NP SPF, which improves the sensor's performance. Thus, the proposed sensor has several merits, such as ease of use, a simple fabrication process, and applicability for temperature monitoring across various applications. Future research will focus on reducing the effects of thermal hysteresis through material optimization and improved manufacturing techniques to provide long-term stability and reliability in practical applications.

5. Acknowledgement

The Ministry of Higher Education (MOHE) funded this study under the Fundamental Research Grant Scheme (FRGS) (FRGS/1/2019/WAB05/UTHM/02/5) (grant No: K170).

6. References

Arjmand, M., Saghafifar, H., Alijanianzadeh, M., & Soltanolkotabi, M. (2017). A sensitive tapered-fiber optic biosensor for the label-free detection of organophosphate pesticides. *Sensors and Actuators B: Chemical*, 249, 523-532.

Bai, Y., Yan, F., Feng, T., Han, W., Zhang, L., Cheng, D., ... & Wen, X. (2019). Temperature fiber sensor based on single longitudinal mode fiber laser in 2 µm band with Sagnac interferometer. *Optical Fiber Technology*, 51, 71-76.

Bolshtyansky, M., Wysocki, P., & Conti, N. (2000). Model of temperature dependence for gain shape of erbium-doped fiber amplifier. *Journal of lightwave technology*, *18*(11), 1533.

Cao, H., & Shu, X. (2017). Miniature all-fiber high temperature sensor based on Michelson interferometer formed with a novel core-mismatching fiber joint. *IEEE Sensors Journa*l, 17(11), 3341-3345.

Chen, F., Jiang, Y., Zhang, L., Jiang, L., & Wang, S. (2018). Fiber optic refractive index and magnetic field sensors based on microhole-induced inline Mach–Zehnder interferometers. *Measurement Science and Technology*, 29(4), 045103.

Chou, Y. L., Wu, C. W., Jhang, R. T., & Chiang, C. C. (2019). A novel optical fiber temperature sensor with polymer-metal alternating structure. *Optics & Laser Technology*, 115, 186-192.

Fried, N. M. (2005). Thulium fiber laser lithotripsy: An in vitro analysis of stone fragmentation using a modulated 110-watt Thulium fiber laser at 1.94 µm. *Lasers in Surgery and Medicine: The Official Journal of the American Society for Laser Medicine and Surgery*, 37(1), 53-58.

Fu, X., Zhang, Y., Wang, Y., Fu, G., Jin, W., & Bi, W. (2020). A temperature sensor based on tapered few mode fiber long-period grating induced by CO2 laser and fusion tapering. *Optics & Laser Technology*, 121, 105825.

Ganeev, R. A. (2019). Characterization of the optical nonlinearities of silver and gold nanoparticles. *Optics and Spectroscopy*, *127*(3), 487-507.

Gonzalez-Reyna, M. A., Alvarado-Mendez, E., Estudillo-Ayala, J. M., Vargas-Rodriguez, E., Sosa-Morales, M. E., Sierra-Hernandez, J. M., & Rojas-Laguna, R. (2015). Laser temperature sensor based on a fiber Bragg grating. *IEEE Photonics Technology Letters*, 27(11), 1141-1144.

Grobnic, D., Smelser, C. W., Mihailov, S. J., & Walker, R. B. (2006). Long-term thermal stability tests at 1000 C of silica fibre Bragg gratings made with ultrafast laser radiation. *Measurement Science and Technology*, 17(5), 1009.

Huang, Y., Zhu, W., Li, Z., Chen, G., Chen, L., Zhou, J., & Yu, J. (2018). High-performance fibre-optic humidity sensor based on a side-polished fibre wavelength selectively coupled with graphene oxide film. *Sensors and actuators B: chemical*, 255, 57-69.

Jachpure, D., Prakash, O., & Vijaya, R. (2024). Saturable absorption in erbium-doped fiber for controlling lasing peaks and their linewidths in fiber laser. *Optical Fiber Technology*, *88*, 104022.

Jung, M., Lee, J., Koo, J., Park, J., Song, Y. W., Lee, K., & Lee, J. H. (2014). A femtosecond pulse fiber laser at 1935 nm using a bulk-structured Bi 2 Te 3 topological insulator. *Optics express*, 22(7), 7865-7874.

Kieu, K. Q., & Mansuripur, M. (2006). Biconical fiber taper sensors. *IEEE photonics technology letters*, 18(21), 2239-2241.

Keller, U. (2000, September). Ultrafast solid-state lasers. In The European Conference on Lasers and Electro-Optics (p. CMB3). *Optica Publishing Group*.

Li, X., Xu, W., Wang, Y., Zhang, X., Hui, Z., Zhang, H., & Al-Sehemi, A. G. (2022). Optical-intensity modulators with PbTe thermoelectric nanopowders for ultrafast photonics. *Applied Materials Today*, 28, 101546.

Li, J., Wu, J., Hao, Q., Huang, K., Yang, K., & Zeng, H. (2023). Wavelength and repetition rate tunable high peak power dissipative soliton resonance in an all polarization maintaining Yb-doped fiber laser. *Optics & Laser Technology*, 162, 109204.

Lu, L., Liang, Z., Wu, L., Chen, Y., Song, Y., Dhanabalan, S. C., & Zhang, H. (2018). Few-layer bismuthene: sonochemical exfoliation, non-linear optics and applications for ultrafast photonics with enhanced stability. *Laser & Photonics Reviews*, 12(1), 1700221.

Lu, Z., Liu, C., Li, C., Ren, J., & Yang, L. (2023). Ultra-High Sensitivity and Temperature-Insensitive Optical Fiber Strain Sensor Based on Dual Air Cavities. *Materials*, 16(8), 3165.

Lin, Y., Gong, Y., Wu, Y., & Wu, H. (2015). Polyimide-coated fiber Bragg grating for relative humidity sensing. *Photonic sensors*, 5, 60-66.

Lin, Q., Hu, Y., Yan, F., Hu, S., Chen, Y., Liu, G., & Chen, Z. (2020). Half-side gold-coated hetero-core fiber for highly sensitive measurement of a vector magnetic field. *Optics Letters*, 45(17), 4746-4749.

Luo, W., Li, X., Meng, J., Wang, Y., & Hong, X. (2021). Surface plasmon resonance sensor based on side-polished D-shaped photonic crystal fiber with split cladding air holes. *IEEE Transactions on Instrumentation and Measurement*, 70, 1-11.

Liao, H. B., Xiao, R. F., Fu, J. S., Yu, P., Wong, G. K. L., & Sheng, P. (1997). Large third-order optical nonlinearity in Au: Si O 2 composite films near the percolation threshold. *Applied Physics Letters*, 70(1), 1-3.

Mądry, M., Alwis, L., Binetti, L., Pajewski, Ł., & Bereś-Pawlik, E. (2019). Simultaneous measurement of temperature and relative humidity using a dual-wavelength erbium-doped fiber ring laser sensor. *IEEE Sensors Journal*, 19(20), 9215-9220.

Matsas, V. J., Newson, T. P., Richardson, D. J., & Payne, D. N. (1992). Self-starting, passively mode-locked fibre ring soliton

DOI: https://doi.org/10.22452/mjs.vol45sp1.5
Malaysian Journal of Science 45 (Special Issue 1): 37-43 (June 2026)

laser exploiting non-linear polarisation rotation. *Electronics Letters*, 28(15), 1391-1393.

Mahmud, N. N. H. E. N., Awang, N. A., & Zulkefli, N. U. H. H. (2022). Supercontinuum generation of gold coated side-polished fiber based-mode-locked pulse. *Optik*, 260, 169074.

Mahmud, N. N. H. E. N., Awang, N. A., Zalkepali, N. U. H. H., Latif, A. A., Muhammad, N. A. M., & Zamri, A. Z. M. (2023). The influence of Au-NP thickness coated on side-polished fiber on the properties of mode-locked erbium-doped fiber laser. *Infrared Physics & Technology*, 130, 104616.

Novoselov, K. S., Geim, A. K., Morozov, S. V., Jiang, D., Katsnelson, M. I., Grigorieva, I. V., & Firsov, A. A. (2005). Two-dimensional gas of massless Dirac fermions in graphene. *Nature*, 438(7065), 197-200.M.

Senosiain, J., Díaz, I., Gastón, A., & Sevilla, J. (2002). High sensitivity temperature sensor based on side-polished optical fiber. *IEEE Transactions on Instrumentation and measurement*, 50(6), 1656-1660.

Sun, Z., Hasan, T., Torrisi, F., Popa, D., Privitera, G., Wang, F., & Ferrari, A. C. (2010). Graphene mode-locked ultrafast laser. *ACS nano*, 4(2), 803-810.

Song, H., Wang, Q., Zhang, Y., & Li, L. (2017). Mode-locked ytterbium-doped all-fiber lasers based on few-layer black phosphorus saturable absorbers. *Optics Communications*, 394, 157-160.

Sharma, A. K., & Gupta, B. D. (2006). Influence of temperature on the sensitivity and signal-to-noise ratio of a fiber-optic surface-plasmon resonance sensor. *Applied optics*, 45(1), 151-161.

Stewart, G., Culshaw, B., Johnstone, W., Whitenett, G., Atherton, K., & McLean, A. (2003). Optical fibre sensors and networks for environmental monitoring. *Management of Environmental Quality: An International Journal*, 14(2), 181-190.

Teng, C., Shao, P., Li, S., Li, S., Liu, H., Deng, H., & Deng, S. (2022). Double-side polished U-shape plastic optical fiber based SPR sensor for the simultaneous measurement of refractive index and temperature. *Optics communications*, 525, 128844.

Trushin, M., Kelleher, E. J., & Hasan, T. (2016). Theory of edge-state optical absorption in two-dimensional transition metal dichalcogenide flakes. *Physical Review B*, 94(15), 155301.

Viegas, D., Goicoechea, J., Santos, J. L., Araújo, F. M., Ferreira, L. A., Arregui, F. J., & Matias, I. R. (2009). Sensitivity improvement of a humidity sensor based on silica nanospheres on a long-period fiber grating. *Sensors*, 9(1), 519-527.

Wu, W., & Liu, X. (2015). Investigation on high temperature characteristics of FBG sensors. *Optik*, 126(20), 2411-2413.

Wang, X., Sun, X., Hu, Y., Zeng, L., Liu, Q., & Duan, J. A. (2022). Highly-sensitive fiber Bragg grating temperature sensors with metallic coatings. *Optik*, 262, 169337.

Zhou, H. S., Honma, I., Komiyama, H., & Haus, J. W. (1994). Controlled synthesis and quantum-size effect in gold-coated nanoparticles. *Physical Review B*, 50(16), 12052.

Zhang, Y., Jin, W., Yu, H. B., Zhang, M., Liao, Y. B., Ho, H. L., & Li, Y. H. (2002). Novel intracavity sensing network based on mode-locked fiber laser. *IEEE Photonics Technology Letters*, 14(9), 1336-1338.

Zainuddin, N. A. A. M., Ariannejad, M. M., Arasu, P. T., Harun, S. W., & Zakaria, R. (2019). Investigation of cladding thicknesses on silver SPR based side-polished optical fiber refractive-index sensor. *Results in Physics*, 13, 102255.

DOI: https://doi.org/10.22452/mjs.vol45sp1.5
Malaysian Journal of Science 45 (Special Issue 1): 37-43 (June 2026)